HHS Public Access

Author manuscript

ACS Synth Biol. Author manuscript; available in PMC 2017 May 20.

Published in final edited form as:

ACS Synth Biol. 2016 May 20; 5(5): 395–404. doi:10.1021/acssynbio.5b00266.

Quantitative Analyses of Core Promoters Enable Precise Engineering of Regulated Gene Expression in Mammalian Cells

Christopher Ede, **Ximin Chen**, **Meng-Yin Lin**, and **Yvonne Y. Chen***

Department of Chemical and Biomolecular Engineering, University of California—Los Angeles, Los Angeles, California 90095, United States

Abstract

Inducible transcription systems play a crucial role in a wide array of synthetic biology circuits. However, the majority of inducible promoters are constructed from a limited set of tried-and-true promoter parts, which are susceptible to common shortcomings such as high basal expression levels (i.e., leakiness). To expand the toolbox for regulated mammalian gene expression and facilitate the construction of mammalian genetic circuits with precise functionality, we quantitatively characterized a panel of eight core promoters, including sequences with mammalian, viral, and synthetic origins. We demonstrate that this selection of core promoters can provide a wide range of basal gene expression levels and achieve a gradient of fold-inductions spanning two orders of magnitude. Furthermore, commonly used parts such as minimal CMV and minimal SV40 promoters were shown to achieve robust gene expression upon induction, but also suffer from high levels of leakiness. In contrast, a synthetic promoter, YB_TATA, was shown to combine low basal expression with high transcription rate in the induced state to achieve significantly higher fold-induction ratios compared to all other promoters tested. These behaviors remain consistent when the promoters are coupled to different genetic outputs and different response elements, as well as across different host-cell types and DNA copy numbers. We apply this quantitative understanding of core promoter properties to the successful engineering of human T cells that respond to antigen stimulation via chimeric antigen receptor signaling specifically under hypoxic environments. Results presented in this study can facilitate the design and calibration of future mammalian synthetic biology systems capable of precisely programmed functionality.

Keywords

mammalian inducible promoters; transcriptional control; mammalian synthetic biology; chimeric antigen receptors; adoptive T-cell therapy

*Corresponding Author: Tel: +1-310-825-2816. ; Email: yvonne.chen@ucla.edu.

Author Contributions

CE, XC, and YYC designed the experiments and analyzed data. CE, XC, and MYL designed and built promoter and reporter constructs. CE and XC performed the experiments. CE and YYC wrote the manuscript.

Supporting Information. Figure S1: Transfection efficiency of plasmids encoding core promoter panels in HEK 293T cells. Figure S2: Comparison of gene expression vs. distance between promoter and start codon in expression plasmids. Figure S3: Population gating strategy for flow cytometry data. Figure S4: sfGFP expression by core promoters in the uninduced state. Figure S5: Gluc output and fold-induction of IL-6–responsive transcription systems in transiently transfected HEK 293T cells. Table S1: List of core promoter sequences. This material is available free of charge on the ACS Publications website at http://pubs.acs.org.

INTRODUCTION

Transcriptional regulatory elements form the foundation of a vast array of synthetic biology systems, ranging from oscillators[1, 2] to memory circuits[3–8] to biocomputers.[9–11] Inducible promoters are typically constructed by linking core promoters to specific enhancers or transcription-factor binding sites (also known as response elements or REs). In this architecture, the RE dictates input-signal specificity and varies with each ligand of interest, whereas the same core promoter can be reused across multiple inducible promoters. As a result, most engineering efforts on transcriptional regulation have focused on the identification and optimization of transcription factors and their associated REs. In particular, research activities in the past decade have enabled the construction of synthetic transcription activators and repressors from zinc-finger (ZF) proteins,[12, 13] transcription activator-like effectors (TALEs),[14–16] and clustered regular interspaced short palindromic repeats (CRISPR)/CRISPR-associated protein 9 (Cas9),[17–21] facilitating the development of novel inducible promoters with completely researcher-specified transcription factors and corresponding REs. Furthermore, the systematic translation of prokaryotic transcription factors and REs to mammalian cells has been demonstrated in recent studies,[22] setting the stage for a rapid expansion of the toolbox for synthetic mammalian transcriptional regulation.

In contrast to the large and growing variety of transcription factors and corresponding REs for mammalian synthetic biology, relatively few options exist in the choice of core promoters[23]. The majority of mammalian inducible promoters reported thus far are constructed from a small selection of core promoters, most prominently the minimal cytomegalovirus (minCMV) promoter.[8, 24–27] Although these tried-and-true promoters have enabled the demonstration of diverse functional outputs, they do not necessarily exhibit optimal regulatory behavior. Furthermore, efforts to compare the performance of different core promoters is complicated by the fact that different studies employ different genetic outputs that vary widely in protein half-life and quantification methods (e.g., fluorescence vs. enzymatic output). These differences can result in drastically different fold-induction measurements even when actual transcription rates are comparable, thus preventing meaningful comparisons across different studies.

As synthetic biology moves toward the development of complex mammalian systems whose robustness is critically dependent on the precise expression level and ligand-responsiveness of inducible transcriptional elements, a quantitative understanding of core promoter properties is needed to facilitate system design and reduce the need for trial and error. Here, we report on the quantitative evaluation of a panel of eight core promoters for mammalian gene expression, including promoters with viral, mammalian, and completely synthetic origins. We demonstrate that the panel of promoters provides a wide range of gene expression levels in the absence of induction and exhibits a gradient of fold-inductions spanning two orders of magnitude. We identify specific core promoters with distinct properties upon induction—i.e., high absolute expression level vs. high fold-change—that may be selectively incorporated into genetic circuits to enable precise functionalities. Finally, we demonstrate the utility of having a quantitative understanding of promoter properties by engineering chimeric antigen receptor (CAR)-expressing T cells that become

responsive to antigen stimulation specifically in hypoxic environments, which are characteristic of solid tumors.[28, 29] Conventional CAR-T cells constitutively express the CAR, resulting in frequent occurrences of on-target, off-tumor toxicity.[30–33] The ability to stringently regulate CAR expression and thus restrict antigen recognition and T-cell activation to the tumor microenvironment could significantly increase the safety profile of T-cell immunotherapy for cancer.

The consistency of our study results across different input signals, genetic outputs, and host-cell types indicates that the core promoter properties elucidated here can guide the design of future biological circuits and facilitate the customization of each system for specific applications of interest.

RESULTS AND DISCUSSION

Panel of Core Promoters Enables Wide Range of Constitutive Mammalian Gene Expression

Optimized genetic circuits and metabolic pathways frequently require precisely calibrated gene expression levels, whether constitutive or regulated by ligand input. In prokaryotic systems, graded gene expression can be achieved through varying the strength of the ribosome-binding site (RBS).[34, 35] Although RBS tuning does not apply to eukaryotic cells, promoters with varying transcription rates can provide an analogously useful toolbox when calibrating synthetic mammalian systems[36]. Core promoters are minimal structures that enable the formation of the initiation complex, and they typically drive basal levels of transcription independently of any associated REs. We characterized a panel of eight core promoters, including minCMV,[27] CMV53 (minCMV with the addition of an upstream GC box),[37] minSV40 (minimal simian virus 40 promoter),[38] miniTK (the −33 to +32 region of the Herpes simplex thymidine kinase promoter),[39] MLP (the −38 to +6 region of the adenovirus major late promoter),[40] pJB42CAT5 (a minimal promoter derived from the human *junB* gene),[41] YB_TATA (a synthetic minimal promoter developed by Benenson and colleagues),[42] and the TATA box alone[43] (Table S1, Supporting Information). The constitutive CMV promoter was also included as reference. These promoters were chosen either for their widespread use in synthetic biology circuits and commercial vectors (e.g., minCMV, minSV40, miniTK, and MLP), or because they had been reported to show robust, inducible activity in human cells (e.g., pJB42CAT5 and YB_TATA). Each promoter was cloned upstream of either *Gaussia* luciferase (Gluc) or superfolder green fluorescent protein (sfGFP) in the absence of any RE. A constitutive CMV promoter driving dsRed-Express was encoded on the same plasmids as the Gluc or sfGFP expression cassette to enable identification of transfected cells in transient-transfection experiments (Figure 1a and Supplementary Text 1, Supporting Information).

DsRed expression patterns in transfected human embryonic kidney (HEK) 293T cells confirmed that transfection efficiency was highly consistent across the constructs tested (Figure S1, Supporting Information). Gluc activity and sfGFP fluorescence measurements indicated that the panel of promoters spanned two to three orders of magnitude in basal gene-expression output, and the relative expression level across promoters remains largely consistent regardless of the type of reporter used (Figure 1b,c). Furthermore, differences in

expression levels were independent of variations in the distance between the promoter and the start codon that resulted from the cloning process (Figure S2, Supporting Information). These results indicate that the choice of core promoters can be used to tune mammalian expression cassettes across a wide range of gene expression levels.

Notably, the most commonly used core promoter—minCMV—is also the leakiest promoter, expressing both Gluc and sfGFP at >15% of the level produced by the strong, constitutive CMV promoter (Figure 1b,c). We investigated whether the observed promoter leakiness was a result of strong gene expression by rare outliers or representative of the overall population. Flow cytometry data are well suited for this comparison, as median fluorescence intensity (MFI) provides a measure of gene expression level within each cell, while population gating (Figure S3, Supporting Information) reveals the proportion of cells that exceeds the binary threshold for detectable gene-expression output. Among dsRed+ (i.e., transfected) cells, % sfGFP+ results showed a smooth gradation across the nine promoters tested, with the majority of the core promoters showing significant leakiness (Figure 1d and Figure S4, Supporting Information). In particular, minCMV was nearly on par with the constitutive CMV promoter in this regard, with 81% of all transfected cells expressing sfGFP from the core promoter in the absence of any RE or induction. In contrast, sfGFP fluorescence intensity among both dsRed+ gated cells (Figure 1c) and dsRed+/sfGFP+ gated cells (Figure 1e) showed a significant gap between the constitutive CMV promoter and the series of core promoters. These results indicate that core promoters such as minCMV and minSV40 drive low-to-moderate levels of gene expression in a large fraction of the population, thus basal expression from these core promoters can serve as a reliable means for tuning constitutive gene expression. Furthermore, these results reveal the limitations of oft-used promoters such as minCMV in applications that require a tightly “off” state in regulated gene expression.

Choice of Core Promoter Significantly Affects Inducibility

Although our results indicate that core promoters can provide a range of constitutive expression levels, the primary utility of core promoters is in the context of inducible transcription systems. The inducibility of a regulated promoter—i.e., the change in gene expression in the presence vs. absence of input signal—is most frequently attributed to the interaction between transcription factors and their corresponding REs. As a result, the most common approach to adjusting promoter inducibility is to vary the sequence, copy number, and/or spacing between RE repeats coupled to a fixed core promoter. However, we hypothesized that the core promoter also plays an essential role in regulated transcription initiation, and set out to quantify the relative inducibility of the panel of core promoters, each coupled to four copies of the same hypoxia-responsive element (HRE) recognized by hypoxia inducible factor (HIF)-1α (Figure 2a and Supplementary Text 2, Supporting Information).

As hypothesized, a significant difference in inducibility and total expression was observed across the panel of core promoters. Regardless of the type of genetic output (Gluc or sfGFP), the minCMV promoter had the largest increase in absolute gene expression when induced, but its fold-change was relatively small due to its high basal expression level (Figure 2b,c). In contrast, the synthetic YB_TATA promoter consistently yielded the highest fold-

induction, owing to a combination of low basal expression and strong increase in absolute expression level upon induction. It should be noted that low basal expression was necessary but not sufficient for high fold-induction (Figure 2d,e). The difference in fold-induction across the promoter panel spanned two orders of magnitude in both reporter systems, indicating that the choice of core promoter has a profound effect on inducibility and can provide an effective means of calibrating inducible transcription systems.

Relative Promoter Inducibility Is Maintained Across Different Host-Cell Types and Associated Response Elements

The observation that both minCMV and minSV40 have relatively low fold-induction is notable given the widespread use of these particular promoter sequences in synthetic inducible promoters. We thus investigated whether this observation was specific to the particular host cell or input signal used in our test system. Results indicate that the relative inducibility among the core promoters is consistent across different host cells and across different REs to which the core promoters are coupled (Figures 3 and 4).

Plasmids encoding the panel of core promoters driving Gluc expression were transiently transfected into HEK 293T, MCF7 breast carcinoma, and Jurkat T-cell lines and quantified for enzymatic output. These human cell lines were chosen to span a range of properties, including adherent vs. non-adherent, epithelial vs. lymphoid, and fetal vs. carcinogenic cell origins. Gene expression level and fold-induction from a given promoter varied across cell lines (Figure 3), which was expected given the three cell lines' differing capacities for plasmid replication, transgene expression, and cellular response to hypoxia. However, for each host-cell type, the relative expression level and fold-induction across the panel of promoters remained remarkably consistent (note similar curve contours across host-cell types in Figure 3). Specifically, minCMV consistently yielded the highest absolute expression level upon induction (Figure 3a), while YB_TATA always achieved the largest fold-induction among all the promoters tested (Figure 3b), regardless of host-cell identity. These results indicate that the relative inducibility among the core promoters is an intrinsic property that holds true across a wide variety of host-cell environments.

We next investigated whether changing the RE to which the core promoter is coupled would alter the inducibility of the resulting transcription unit. JRE-IL6 is an IL-6–responsive transcription-factor–binding site found in the human *junB* gene.[41] We constructed IL-6–inducible Gluc reporters by coupling JRE-IL6 to the panel of core promoters (Supplementary Text 3, Supporting Information), and quantified luciferase activity in transiently transfected HEK 293T cells (Figure 4 and Figure S5, Supporting Information). Consistent with observations made in the hypoxia-responsive system, minCMV resulted in high absolute gene expression levels upon induction (Figure 4a), but YB_TATA remained superior in fold-induction (Figure 4b). A prominent difference between the hypoxia- and IL-6–responsive systems was the absolute expression level achieved by pJB42CAT5, which exceeded that of any other promoter tested upon IL-6 induction (Figure 4a and Figure S5a, Supporting Information). pJB42CAT5 was derived from the promoter naturally coupled to the JRE-IL6 response element in the *junB* gene.[41] Therefore, the robust IL-6–induced gene expression from pJB42CAT5 may reflect evolutionary optimization of the natural *junB*

expression cassette. However, even pJB42CAT5 did not match YB_TATA in fold-induction. For all promoters, absolute gene expression and fold-induction plateaued at 20 ng/ml IL-6, indicating that the relatively modest induction ratio observed for promoters such as minCMV was not a result of insufficient ligand input (Figure 4b and Figure S5b, Supporting Information). These results confirm that properties such as robust gene expression for minCMV and large fold-induction for YB_TATA are independent of the specific input signal and response element coupled to the promoter.

Given minCMV's robust gene expression upon induction, its limited fold-induction is largely a result of high basal expression. Since basal expression could be tuned by adjusting gene copy numbers, we examined whether changing the plasmid input during transient transfection or stably integrating the gene expression cassette would significantly affect the inducibility of the core promoters. HEK 293T cells transiently transfected with a range of plasmid input concentrations showed higher fold-inductions at lower plasmid input levels (Figure 5a). A potential explanation for this inverse relationship between fold-induction and plasmid input is that at lower copy numbers, there are fewer promoters to compete for the pool of transcription factor molecules, thus each promoter is more likely to be productively induced. Nevertheless, the relative inducibility across different promoters remained consistent, and minCMV showed only slight improvements in fold-induction at low plasmid input levels, indicating that the intrinsic properties of each core promoter is the dominant determining factor on inducibility.

We next evaluated whether stably integrated expression cassettes would exhibit significantly altered behaviors compared to ectopic plasmids. HEK 293T cells were stably integrated with hypoxia-inducible sfGFP expression cassettes via lentiviral transduction, and transduced cells were subjected to the same culturing conditions as the transiently transfected cells shown in Figure 2. Although stably integrated cells showed smaller fold-inductions compared to transiently transfected samples, stably integrated minCMV still yielded robust gene expression while YB_TATA consistently achieved the largest fold-induction (Figure 5b,c). Therefore, we conclude that the observed behaviors are maintained across genomic and ectopic gene expression contexts.

YB_TATA Combines High Transcription Rate with Low Basal Expression to Achieve Superior Inducibility

To understand the quantitative basis of the core promoters' behaviors, we examined the dynamics of transcription output over a period of 24 hours. The results demonstrated that core promoters vary significantly in transcription rates upon induction, with YB_TATA combining high transcription rate in the induced state with low leakiness in the uninduced state to achieve uniquely high sensitivity to the cognate input signal (Figure 6).

In the absence of induction, luciferase output for each promoter increased exponentially over time and proportionately to each other, resulting in linear, parallel curves on the log-scale plot shown in Figure 6a. Transcription output at any given time is the product of transcripts generated per cell multiplied by cell number, the latter of which changes over time with cell growth. Given that Gluc has a half-life of 6 days in culture medium,[44] the protein output measured at each time point reflects transcription output integrated over the production time

period, with negligible protein degradation during the 24-hour observation window. The pattern of Gluc output observed in the absence of induction (Figure 6a) was consistent with constant transcription rate coupled to exponential cell growth. The relative transcription rate for each promoter can be calculated by normalizing the output of each core promoter to that of the constitutive CMV promoter at each time point. Results indicated that minCMV and YB_TATA each drove gene expression at a constant rate that was 19.9% ± 2.6% and 1.4% ± 0.1% of the constitutive CMV promoter's expression rate, respectively, consistent with the behavior observed in Figure 1b.

Under hypoxic-mimetic culturing conditions generated with the addition of dimethyloxalylglycine (DMOG; see Materials and Methods), the constitutive CMV promoter maintained the same exponential luciferase production profile as under normoxic conditions (Figure 6b). In contrast, the inducible promoters started with low transcription rates that increased gradually upon hypoxia induction, resulting in non-linear increases in luciferase output on the log-scale plot over the first 8–10 hours (Figure 6b). Notably, minCMV and YB_TATA demonstrated similar ramp-up time in transcription rate, and their steady-state transcription rates under hypoxia induction were nearly identical as indicated by similar radiance levels after 12 hours. In contrast, minSV40 had a significantly lower maximum transcription rate than minCMV despite having a similar basal expression level (Figure 6a,b), leading to the lowest fold-induction among the three core promoters (Figure 6c).

These results confirm that the high fold-induction observed with YB_TATA is a result of high transcription rate in the induced state coupled to low basal expression in the uninduced state. This combination enables YB_TATA to achieve a uniquely responsive induction profile that suggests potential utility in applications requiring stringent gene-expression regulation (Figures 2b,c and 6c).

Rationally Designed Inducible Promoter Enables Antigen-Responsive T-cell Activation Specifically in Hypoxic Environments

A quantitative understanding of different core promoters facilitates the construction of novel biological systems. Here, we applied our findings to the engineering of smart T cells that respond to antigen stimulation specifically under hypoxia, a condition that characterizes solid-tumor microenvironments. Adoptive T-cell therapy—a treatment strategy in which T cells are isolated from cancer patients, genetically modified to express tumor-targeting receptors, expanded *ex vivo*, and then re-infused into the same patient— has shown remarkable curative potential against advanced cancers.[31, 45–48] However, off-tumor toxicity, which occurs when T cells kill non-tumor cells that express tumor-associated antigens, has resulted in severe side effects, including patient deaths.[32, 33] Off-tumor toxicity could potentially be prevented by placing the expression of tumor-targeting receptors under the control of an inducible promoter that is specifically triggered in the tumor microenvironment, such that T cells could only respond to antigen stimulation if the antigen were present at specific locations characterized by disease signatures. Rapid cell proliferation in the absence of sufficient blood flow results in low local oxygen concentration, making hypoxia a marker for a wide variety of solid tumors.[28, 29] We thus

aimed to construct a hypoxia-inducible chimeric antigen receptor (CAR) expression system to restrict antigen-responsive T-cell activation to hypoxic environments.

CARs are synthetic T-cell receptors that redirect T-cell specificity toward researcher-specified target antigens.[49] It has been shown that T-cell activation triggered by antigen-receptor binding can occur in the presence of a single antigen molecule.[50, 51] Therefore, we hypothesized that effective restriction of T-cell activation to hypoxic environments requires a hypoxia-inducible system with minimal basal CAR expression under normoxia. To validate this hypothesis, we cloned a CD19-targeting CAR behind both HREx4-minCMV and HREx4- YB_TATA inducible promoters, and included the CD19 CAR expressed from a constitutive EF1α promoter as positive control. Each CAR construct was evaluated in transiently transfected Jurkat cells, and both minCMV and YB_TATA resulted in hypoxia-responsive upregulation of CD19 CAR expression on the cell surface (Figure 7a). However, minCMV resulted in robust CAR expression even under normoxic culturing conditions, thus limiting the fold-change in CAR expression upon hypoxia induction. When co-cultured with CD19+ K562 target cells, Jurkat cells that constitutively expressed the CD19 CAR were efficiently activated by antigen stimulation regardless of environmental oxygen levels, as indicated by robust surface expression of the activation marker CD69 (Figure 7b). Jurkat cells expressing the CD19 CAR from the HREx4-minCMV promoter also showed antigen-specific CD69 upregulation under both normoxia and hypoxia, indicating that high basal CAR expression from the minCMV promoter prevented effective restriction of T-cell activation to hypoxic environments. In contrast, the HREx4-YB_TATA promoter successfully limited CAR expression and the resulting antigen-stimulated T-cell activation to hypoxic environments, thus enabling selective T-cell response to antigen presentation.

Conclusion

Inducible transcription units have played a critical role in diverse synthetic biology circuits, and the ability to calibrate the transcriptional output and responsiveness of inducible promoters can greatly facilitate the construction of novel biological systems. In this study, we systematically characterized the behavior of eight core promoters coupled to different response elements and genetic outputs, yielding quantitative data on basal expression and fold-induction across different host-cell types and input signals.

To date, the majority of mammalian inducible transcription units have been constructed using the minCMV promoter. The success of the minCMV promoter may be attributed to the large absolute increase in gene expression that can be obtained upon induction (Figure 2b,c). Across different input signals, genetic outputs, and host-cell types, minCMV consistently responds to induction with robust upregulation of gene expression. Such a promoter is particularly useful in applications in which the genetic output must be present at high levels to produce the desired signal, such as memory circuits that have a high trigger threshold and require positive feedback to remain in the “on” state.[7, 8]

However, a less publicized feature of minCMV is its leakiness, with over 80% of transfected cells expressing detectable reporter output in the absence of induction (Figure 1d). This property limits the utility of minCMV in applications that require minimal gene expression in the uninduced state, such as suicide gene expression or T-cell activation regulation. The

remarkably high degree of leakiness that characterizes the most commonly used core promoters has likely constrained the type of mammalian genetic circuits achievable to date, as it has in our own experience with engineering human T cells.

In this study, we observed that a synthetic promoter, YB_TATA, has the combined properties of low leakiness and high transcription rate upon induction, resulting in significantly higher fold-induction compared to the other minimal promoters characterized in this study. This promoter, which was developed by Benenson and colleagues,[42] consists of a 25-bp sequence containing a TATA box with flanking spacers. Although the mechanistic basis of YB_TATA's superior inducibility remains to be elucidated, this compact promoter can be easily incorporated into synthetic genetic circuits that require minimal gene expression in the uninduced state. By placing CAR expression under the control of YB_TATA coupled to hypoxia-responsive elements, we successfully engineered human Jurkat T cells to respond to antigen stimulation only when the antigen is present in a hypoxic environment. Such a conditional T-cell activation system could increase the specificity of adoptive T-cell therapy against solid tumors, which are frequently characterized by hypoxic growth. It was notable that the conditional activation of T cells could not be achieved with minCMV, whose leakiness enabled robust antigen-stimulated T-cell activation even under normoxic environments.

Based on the promoter properties quantified in this study, informed decisions can be made in the selection of core promoters during the construction of future mammalian synthetic biology circuits. Strategies such as adjusting the number, sequence, and spacing of response elements coupled to the core promoter can be combined with the choice of core promoter to further refine the expression level and inducibility of transcription units, thus enabling the development of robust mammalian systems for diverse applications ranging from metabolic engineering to cell-based therapy.

METHODS

Plasmid Generation

DsRed-Express was cloned into pcDNA3.1(+) (Invitrogen, Carlsbad, CA) via the NheI and PmeI sites. Core and inducible promoters driving Gluc or sfGFP followed by bGH polyA signal were subsequently inserted upstream of CMV-DsRed via the BglII and NruI sites by either digestion/ligation cloning or Gibson assembly. Gluc was obtained from pCMV Gluc 2 (New England Biolabs, Ipswich, MA) and sfGFP was obtained from pUC-msfGFP (generous gift from Dr. Pamela Silver, Harvard Medical School). The minCMV, minSV40, MLP, and miniTK sequences were obtained from p5HRE/GFP[27] (Addgene, Cambridge, MA), pGL3-Promoter (Promega, Madison, WI), pGL4.31 (Promega), and pGluc Mini-TK2 (New England Biolabs), respectively. The remaining promoter sequences were obtained from the references cited in the text. All core promoter sequences are listed in Supporting Information Table S1. A hypoxia response element (HRE) with the sequence GACCTTGAGTACGTGCGTCTCTGCACGTATG was designed based on the consensus sequences found by Schödel *et al.*[52] The JRE-IL-6 response element (GCGCTTCCTGACAGTGACGCGAGCCG) was obtained from Ref. 41. The CD19 CAR was constructed by Gibson assembly using DNA fragments encoding the FLAG tag

(DYKDDDDK), CD19 scFv derived from the FMC63 monoclonal antibody,[53] an IgG4-derived extracellular spacer, the CD28 transmembrane domain, and the cytoplasmic domains of 4-1BB and CD3 zeta. For stable integration, HREx4-promoter-sfGFP cassettes were transferred to the epHIV7 lentiviral expression vector[54] by digestion-ligation cloning, and truncated epidermal growth factor (EGFRt) expressed by a constitutive EF1α promoter was included on the same vector to enable identification of transduced cells. All DNA fragments were either chemically synthesized 18 or PCR-amplified from existing plasmids. All DNA syntheses were performed by Integrated DNA Technologies (Coralville, IA). Plasmids were sequence-verified by Retrogen (San Diego, CA). Annotated sequences for three representative plasmids—YB_TATA-sfGFP, HREx4- YB_TATA-sfGFP, and JREIL6x4-YB_TATA-sfGFP—are provided in Supplementary Texts 1 through 3, respectively.

Cell-Line Maintenance

HEK 293T, MCF7, and Jurkat Clone E-6 cells were obtained from ATCC (Manassas, VA). K562 cells were a generous gift from Dr. Michael C. Jensen (Seattle Children's Research Institute). All cells were grown in either high-glucose DMEM (MCF7 and HEK 293T; HyClone, Logan, UT) or RPMI (Jurkat and K562; Lonza, Walkersville, MA) supplemented with 10% heat inactivated FBS (HI-FBS; Life Technologies, Grand Island, NY,) at 37°C, 100% humidity and 5% CO2. Anaerobic conditions were achieved by placing culture plates in an air-sealed container together with anaerobic atmosphere generation bags (Sigma-Aldrich, St. Louis, MO) in the 37°C incubator. Hypoxic conditions were achieved by placing culture plates in a sealed hypoxic chamber connected to a gas cylinder containing 1% oxygen, 5% CO_2, 94% N_2. Air inlet and outlet valves were controlled by an electric twin timer programmed to flush the system with 1% oxygen mixture for 2 min every hour at a flow rate sufficient for complete air replacement in the chamber. A water tray was included in both anaerobic and hypoxic chambers to provide humidification.

Cell Transfection

MCF7 cells seeded at 5×10^3 cells/well in 96-well plates were transfected with 10 ng DNA and 13.5 nmol linear polyethylenimine (PEI, 25kDa; Polysciences, Warrington, PA) per well. Unless otherwise stated, HEK 293T cells seeded at 8×10^3 or 5×10^4 cells/well in 96- or 24-well plates, respectively, were transfected with 10 ng DNA/1×10^3 cells and 0.06 nmol PEI/ng DNA. For the experiment with varying DNA input, HEK 293T cells were seeded at 2.5×10^4 cells/well in 48-well plates, and transfected with 31.25, 125, 187.5, or 250 ng of plasmids encoding hypoxia-inducible promoter driving the expression of sfGFP. The pcDNA3.1(+) plasmid (Invitrogen) was added to each transfection sample to bring the total plasmid input to 250 ng per well, and 0.06 nmol PEI/ng DNA was used. Jurkat cells were transfected using the Amaxa Cell Line Nucleofector Kit V (Lonza), with 5 μg of plasmid DNA and 5×10^6 cells per nucleofection following the manufacturer's protocols.

Lentivirus Production and Cell Transduction

HEK 293T cells seeded in T25 cell-culture flasks at 1.5×10^6 cells in 10 ml DMEM + 10% HI-FBS media were transfected using linear PEI. Six hours post-transfection, cells were washed with 10 ml of 1X-phosphate buffered saline without magnesium and calcium (PBS) (Lonza) and supplemented with fresh media containing 60 mM sodium butyrate (Sigma-

Aldrich). Viral supernatant was collected 48 hours after media change, and cell debris was removed from the supernatant by centrifugation at 10,000 rpm for 10 min at 4°C, followed by filtration through a 0.45 μM membrane (Corning, Durham, NC). Untransfected HEK 293T cells were incubated in duplicate in a 12-well plate with 1.5 ml of viral supernatant for 48 hours, then washed with PBS and cultured in a T25 cell-culture flask in fresh DMEM + 10% HI-FBS for 7 days prior to being used for gene expression experiments.

Gaussia Luciferase Assay

Cells were transiently transfected and incubated at 37°C for 24 hours. For hypoxia-induction studies, transfected cells were incubated for 5 hours under standard conditions followed by a 24-hour incubation in anaerobic or hypoxic chambers as indicated. For each construct, three separate wells were transfected in parallel for HEK 293T and MCF7 cells. In case of Jurkat cells, three wells were seeded in parallel originating from the same nucleofected culture. Luciferase activity was determined from diluted samples using the BioLux® Gaussia Luciferase Kit (New England Biolabs) in combination with a Modulus single-tube luminometer (Turner Biosystems, Sunnyvale, CA) or Synergy H1 hybrid plate reader (BioTek, Winooski, VT) with a 5-sec integration time. Background luminescence measured from the supernatant of mock-transfected cells was subtracted from the raw luminescence values. Fold-induction was calculated by dividing the background-subtracted luminescence values of each induced sample by the average value of the three corresponding uninduced samples.

T-cell Activation and Immunostaining

Jurkat human T cells were transiently transfected and incubated under standard conditions for 5 hours at 37°C, followed by co-culturing in the hypoxic chamber with either parental or CD19+ K562 target cells at an effector-to-target ratio of 2:1. Cells were co-incubated for 24 hours at 37°C, then harvested and surface-stained with fluorophore-conjugated antibodies targeting CD69 (FN5O; BioLegend, San Diego, CA). CAR expression was quantified by surface staining with a mouse anti-FLAG antibody (M2, Sigma-Aldrich) followed by a secondary, AlexaFluor 647-conjugated anti-mouse IgG antibody (Life Technologies). Stained samples were analyzed by flow cytometry as described below.

Flow Cytometry

Cells were harvested 24 hours post transfection (for basal expression studies) or post induction (for inducible expression studies), washed, and resuspended in DPBS (Lonza) supplemented with 2% heat-inactivated FBS (Gibco, Waltham, MA). Samples were analyzed using a MACSQuant® YVB flow cytometer equipped with 405-, 488-, and 561-nm lasers (Miltenyi Biotec, San Diego, CA). Flow data were analyzed with the FlowJo Data Analysis software (TreeStar, Ashland, OR). Cells were gated for viable, singlet, dsRed+ (transfected) population prior to quantification for sfGFP, FLAG or CD69 expression (Figure S3, Supporting Information).

Induction Dynamics and Mathematical Modeling

For IL-6 dose response dynamics, transfected HEK 293T cells were incubated for 5 hours at 37°C before the indicated concentrations of recombinant IL-6 (BioLegend) were added to the culture media. After overnight incubation at 37°C, luciferase activity was measured as described above. For each promoter, fold-induction was calculated by dividing the radiance value of each induced sample by the average radiance of three mock-induced samples, which received PBS instead of IL-6. For induction time-course experiments, transfected HEK 293T cells were incubated overnight at 37°C before inducing hypoxia response by adding 2 mM DMOG (prepared as 250 mM stock solution in dimethyl sulfoxide (DMSO); Caiman Chemical, Ann Arbor, MI). DMOG increases HIF levels by inhibiting prolyl and asparaginyl hydroxylase, thus generating a hypoxia-mimetic environment that can be sampled at multiple time points without disrupting the hypoxic nature of the cell culture.[55] An equal volume of DMSO (Sigma-Aldrich) was added to the negative-control wells. From each well, 10 μl of supernatant were collected at the indicated time points, with the 0-hour time point collected immediately before induction. Luciferase activity was quantified as described above. Fold-induction was calculated by dividing the radiance value of each induced sample by the average radiance of the three mock-induced samples obtained at the corresponding time point. The resulting plots for $f(x)=\frac{\Delta(average\ fold\ change)}{\Delta(time)}$ were fitted to a Hill equation with four parameters using the global curve fit function of Sigma Plot (Systat Software Inc., San Jose, CA): $y(x)=\frac{ax^n}{b^n x^n}+y_0$, where = $y_{max} - y_0$, **n** is the Hill co-efficient, and **b** is the value of × when $y(x) = 0.5 * y_{max}$. Fold change was normalized to the uninduced state at the 0-hour time point—i.e., $y(0)$ was defined as 1.

Supplementary Material

Refer to Web version on PubMed Central for supplementary material.

Acknowledgments

This work was supported by the National Institutes of Health (5DP5OD012133; grant to YYC) and the UCLA Henry Samueli School of Engineering and Applied Science. The authors thank Eugenia Zah and Michael H. Lorenzini for their technical assistance.

References

1. Elowitz MB, Leibler S. A synthetic oscillatory network of transcriptional regulators. Nature. 2000; 403:335–338. [PubMed: 10659856]
2. Prindle A, Selimkhanov J, Li H, Razinkov I, Tsimring LS, Hasty J. Rapid and tunable post-translational coupling of genetic circuits. Nature. 2014; 508:387–391. [PubMed: 24717442]
3. Siuti P, Yazbek J, Lu TK. Synthetic circuits integrating logic and memory in living cells. Nat Biotechnol. 2013; 31:448–452. [PubMed: 23396014]
4. Bonnet J, Subsoontorn P, Endy D. Rewritable digital data storage in live cells via engineered control of recombination directionality. Proc Natl Acad Sci U S A. 2012; 109:8884–8889. [PubMed: 22615351]
5. Ajo-Franklin CM, Drubin DA, Eskin JA, Gee EP, Landgraf D, Phillips I, Silver PA. Rational design of memory in eukaryotic cells. Genes Dev. 2007; 21:2271–2276. [PubMed: 17875664]
6. Ham TS, Lee SK, Keasling JD, Arkin AP. Design and construction of a double inversion recombination switch for heritable sequential genetic memory. PLoS One. 2008; 3:e2815. [PubMed: 18665232]

7. Burrill DR, Silver PA. Synthetic circuit identifies subpopulations with sustained memory of DNA damage. Genes Dev. 2011; 25:434–439. [PubMed: 21363961]
8. Burrill DR, Inniss MC, Boyle PM, Silver PA. Synthetic memory circuits for tracking human cell fate. Genes Dev. 2012; 26:1486–1497. [PubMed: 22751502]
9. Friedland AE, Lu TK, Wang X, Shi D, Church G, Collins JJ. Synthetic gene networks that count. Science. 2009; 324:1199–1202. [PubMed: 19478183]
10. Auslander S, Auslander D, Muller M, Wieland M, Fussenegger M. Programmable single-cell mammalian biocomputers. Nature. 2012; 487:123–127. [PubMed: 22722847]
11. Daniel R, Rubens JR, Sarpeshkar R, Lu TK. Synthetic analog computation in living cells. Nature. 2013; 497:619–623. [PubMed: 23676681]
12. Choo Y, Sanchez-Garcia I, Klug A. In vivo repression by a site-specific DNA-binding protein designed against an oncogenic sequence. Nature. 1994; 372:642–645. [PubMed: 7990954]
13. Khalil AS, Lu TK, Bashor CJ, Ramirez CL, Pyenson NC, Joung JK, Collins JJ. A synthetic biology framework for programming eukaryotic transcription functions. Cell. 2012; 150:647–658. [PubMed: 22863014]
14. Perez-Pinera P, Ousterout DG, Brunger JM, Farin AM, Glass KA, Guilak F, Crawford GE, Hartemink AJ, Gersbach CA. Synergistic and tunable human gene activation by combinations of synthetic transcription factors. Nat Methods. 2013; 10:239–242. [PubMed: 23377379]
15. Sanjana NE, Cong L, Zhou Y, Cunniff MM, Feng G, Zhang F. A transcription activator-like effector toolbox for genome engineering. Nat Protoc. 2012; 7:171–192. [PubMed: 22222791]
16. Garg A, Lohmueller JJ, Silver PA, Armel TZ. Engineering synthetic TAL effectors with orthogonal target sites. Nucleic Acids Res. 2012; 40:7584–7595. [PubMed: 22581776]
17. Esvelt KM, Mali P, Braff JL, Moosburner M, Yaung SJ, Church GM. Orthogonal Cas9 proteins for RNA-guided gene regulation and editing. Nat Methods. 2013; 10:1116–1121. [PubMed: 24076762]
18. Qi LS, Larson MH, Gilbert LA, Doudna JA, Weissman JS, Arkin AP, Lim WA. Repurposing CRISPR as an RNA-guided platform for sequence-specific control of gene expression. Cell. 2013; 152:1173–1183. [PubMed: 23452860]
19. Gilbert LA, Larson MH, Morsut L, Liu Z, Brar GA, Torres SE, Stern-Ginossar N, Brandman O, Whitehead EH, Doudna JA, Lim WA, Weissman JS, Qi LS. CRISPR-mediated modular RNA-guided regulation of transcription in eukaryotes. Cell. 2013; 154:442–451. [PubMed: 23849981]
20. Perez-Pinera P, Kocak DD, Vockley CM, Adler AF, Kabadi AM, Polstein LR, Thakore PI, Glass KA, Ousterout DG, Leong KW, Guilak F, Crawford GE, Reddy TE, Gersbach CA. RNA-guided gene activation by CRISPR-Cas9-based transcription factors. Nat Methods. 2013; 10:973–976. [PubMed: 23892895]
21. Zetsche B, Volz SE, Zhang F. A split-Cas9 architecture for inducible genome editing and transcription modulation. Nat Biotechnol. 2015; 33:139–142. [PubMed: 25643054]
22. Stanton BC, Siciliano V, Ghodasara A, Wroblewska L, Clancy K, Trefzer AC, Chesnut JD, Weiss R, Voigt CA. Systematic transfer of prokaryotic sensors and circuits to mammalian cells. ACS Synth Biol. 2014; 3:880–891. [PubMed: 25360681]
23. Lanza AM, Cheng JK, Alper HS. Emerging synthetic biology tools for engineering mammalian cell systems and expediting cell line development. Curr Opin Chem Eng. 2012; 1:403–410.
24. Gossen M, Bujard H. Tight control of gene expression in mammalian cells by tetracycline-responsive promoters. Proc Natl Acad Sci U S A. 1992; 89:5547–5551. [PubMed: 1319065]
25. Gitzinger M, Kemmer C, El-Baba MD, Weber W, Fussenegger M. Controlling transgene expression in subcutaneous implants using a skin lotion containing the apple metabolite phloretin. Proc Natl Acad Sci U S A. 2009; 106:10638–10643. [PubMed: 19549857]
26. Li Y, Jiang Y, Chen H, Liao W, Li Z, Weiss R, Xie Z. Modular construction of mammalian gene circuits using TALE transcriptional repressors. Nat Chem Biol. 2015; 11:207–213. [PubMed: 25643171]
27. Shibata T, Giaccia AJ, Brown JM. Development of a hypoxia-responsive vector for tumor-specific gene therapy. Gene Ther. 2000; 7:493–498. [PubMed: 10757022]
28. Wilson WR, Hay MP. Targeting hypoxia in cancer therapy. Nat Rev Cancer. 2011; 11:393–410. [PubMed: 21606941]

29. Brahimi-Horn MC, Chiche J, Pouyssegur J. Hypoxia and cancer. J Mol Med (Berl). 2007; 85:1301–1307. [PubMed: 18026916]
30. Brentjens R, Yeh R, Bernal Y, Riviere I, Sadelain M. Treatment of chronic lymphocytic leukemia with genetically targeted autologous T cells: case report of an unforeseen adverse event in a phase I clinical trial. Molecular therapy : the journal of the American Society of Gene Therapy. 2010; 18:666–668. [PubMed: 20357779]
31. Kochenderfer JN, Dudley ME, Feldman SA, Wilson WH, Spaner DE, Maric I, Stetler-Stevenson M, Phan GQ, Hughes MS, Sherry RM, Yang JC, Kammula US, Devillier L, Carpenter R, Nathan DA, Morgan RA, Laurencot C, Rosenberg SA. B-cell depletion and remissions of malignancy along with cytokine-associated toxicity in a clinical trial of anti-CD19 chimeric-antigen-receptor-transduced T cells. Blood. 2012; 119:2709–2720. [PubMed: 22160384]
32. Morgan RA, Yang JC, Kitano M, Dudley ME, Laurencot CM, Rosenberg SA. Case report of a serious adverse event following the administration of T cells transduced with a chimeric antigen receptor recognizing ERBB2. Molecular therapy : the journal of the American Society of Gene Therapy. 2010; 18:843–851. [PubMed: 20179677]
33. Linette GP, Stadtmauer EA, Maus MV, Rapoport AP, Levine BL, Emery L, Litzky L, Bagg A, Carreno BM, Cimino PJ, Binder-Scholl GK, Smethurst DP, Gerry AB, Pumphrey NJ, Bennett AD, Brewer JE, Dukes J, Harper J, Tayton-Martin HK, Jakobsen BK, Hassan NJ, Kalos M, June CH. Cardiovascular toxicity and titin cross-reactivity of affinity-enhanced T cells in myeloma and melanoma. Blood. 2013; 122:863–871. [PubMed: 23770775]
34. Salis HM, Mirsky EA, Voigt CA. Automated design of synthetic ribosome binding sites to control protein expression. Nat Biotechnol. 2009; 27:946–950. [PubMed: 19801975]
35. Kushwaha M, Salis HM. A portable expression resource for engineering cross-species genetic circuits and pathways. Nat Commun. 2015; 6:7832. [PubMed: 26184393]
36. Ferreira JP, Peacock RW, Lawhorn IE, Wang CL. Modulating ectopic gene expression levels by using retroviral vectors equipped with synthetic promoters. Syst Synth Biol. 2011; 5:131–138. [PubMed: 23205156]
37. Mahmoud L, Al-Saif M, Amer HM, Sheikh M, Almajhdi FN, Khabar KS. Green fluorescent protein reporter system with transcriptional sequence heterogeneity for monitoring the interferon response. J Virol. 2011; 85:9268–9275. [PubMed: 21752918]
38. Byrne BJ, Davis MS, Yamaguchi J, Bergsma DJ, Subramanian KN. Definition of the Simian Virus-40 Early Promoter Region and Demonstration of a Host Range Bias in the Enhancement Effect of the Simian Virus-40 72-Base-Pair Repeat. P Natl Acad Sci-Biol. 1983; 80:721–725.
39. McKnight SL, Gavis ER, Kingsbury R, Axel R. Analysis of transcriptional regulatory signals of the HSV thymidine kinase gene: identification of an upstream control region. Cell. 1981; 25:385–398. [PubMed: 6269744]
40. Lewis ED, Manley JL. Control of adenovirus late promoter expression in two human cell lines. Mol Cell Biol. 1985; 5:2433–2442. [PubMed: 2942764]
41. Nakajima K, Kusafuka T, Takeda T, Fujitani Y, Nakae K, Hirano T. Identification of a novel interleukin-6 response element containing an Ets-binding site and a CRE-like site in the junB promoter. Mol Cell Biol. 1993; 13:3027–3041. [PubMed: 8386318]
42. Hansen J, Mailand E, Swaminathan KK, Schreiber J, Angelici B, Benenson Y. Transplantation of prokaryotic two-component signaling pathways into mammalian cells. Proc Natl Acad Sci U S A. 2014; 111:15705–15710. [PubMed: 25331891]
43. Starr DB, Hawley DK. TFIID binds in the minor groove of the TATA box. Cell. 1991; 67:1231–1240. [PubMed: 1760847]
44. Wurdinger T, Badr C, Pike L, de Kleine R, Weissleder R, Breakefield XO, Tannous BA. A secreted luciferase for ex vivo monitoring of in vivo processes. Nat Methods. 2008; 5:171–173. [PubMed: 18204457]
45. Brentjens RJ, Davila ML, Riviere I, Park J, Wang X, Cowell LG, Bartido S, Stefanski J, Taylor C, Olszewska M, Borquez-Ojeda O, Qu J, Wasielewska T, He Q, Bernal Y, Rijo IV, Hedvat C, Kobos R, Curran K, Steinherz P, Jurcic J, Rosenblat T, Maslak P, Frattini M, Sadelain M. CD19-targeted T cells rapidly induce molecular remissions in adults with chemotherapy-refractory acute lymphoblastic leukemia. Sci Transl Med. 2013; 5:177ra138.

46. Davila ML, Riviere I, Wang X, Bartido S, Park J, Curran K, Chung SS, Stefanski J, Borquez-Ojeda O, Olszewska M, Qu J, Wasielewska T, He Q, Fink M, Shinglot H, Youssif M, Satter M, Wang Y, Hosey J, Quintanilla H, Halton E, Bernal Y, Bouhassira DC, Arcila ME, Gonen M, Roboz GJ, Maslak P, Douer D, Frattini MG, Giralt S, Sadelain M, Brentjens R. Efficacy and toxicity management of 19–28z CAR T cell therapy in B cell acute lymphoblastic leukemia. Sci Transl Med. 2014; 6:224ra225.
47. Kalos M, Levine BL, Porter DL, Katz S, Grupp SA, Bagg A, June CH. T cells with chimeric antigen receptors have potent antitumor effects and can establish memory in patients with advanced leukemia. Sci Transl Med. 2011; 3:95ra73.
48. Maude SL, Frey N, Shaw PA, Aplenc R, Barrett DM, Bunin NJ, Chew A, Gonzalez VE, Zheng Z, Lacey SF, Mahnke YD, Melenhorst JJ, Rheingold SR, Shen A, Teachey DT, Levine BL, June CH, Porter DL, Grupp SA. Chimeric antigen receptor T cells for sustained remissions in leukemia. N Engl J Med. 2014; 371:1507–1517. [PubMed: 25317870]
49. Srivastava S, Riddell SR. Engineering CAR-T cells: Design concepts. Trends Immunol. 2015; 36:494–502. [PubMed: 26169254]
50. Sykulev Y, Joo M, Vturina I, Tsomides TJ, Eisen HN. Evidence that a single peptide-MHC complex on a target cell can elicit a cytolytic T cell response. Immunity. 1996; 4:565–571. [PubMed: 8673703]
51. Purbhoo MA, Irvine DJ, Huppa JB, Davis MM. T cell killing does not require the formation of a stable mature immunological synapse. Nat Immunol. 2004; 5:524–530. [PubMed: 15048111]
52. Schodel J, Oikonomopoulos S, Ragoussis J, Pugh CW, Ratcliffe PJ, Mole DR. High-resolution genome-wide mapping of HIF-binding sites by ChIP-seq. Blood. 2011; 117:e207–217. [PubMed: 21447827]
53. Nicholson IC, Lenton KA, Little DJ, Decorso T, Lee FT, Scott AM, Zola H, Hohmann AW. Construction and characterisation of a functional CD19 specific single chain Fv fragment for immunotherapy of B lineage leukaemia and lymphoma. Mol Immunol. 1997; 34:1157–1165. [PubMed: 9566763]
54. Yam PY, Li S, Wu J, Hu J, Zaia JA, Yee JK. Design of HIV vectors for efficient gene delivery into human hematopoietic cells. Molecular therapy : the journal of the American Society of Gene Therapy. 2002; 5:479–484. [PubMed: 11945076]
55. Asikainen TM, Ahmad A, Schneider BK, Ho WB, Arend M, Brenner M, Gunzler V, White CW. Stimulation of HIF-1alpha, HIF-2alpha, and VEGF by prolyl 4-hydroxylase inhibition in human lung endothelial and epithelial cells. Free Radic Biol Med. 2005; 38:1002–1013. [PubMed: 15780758]

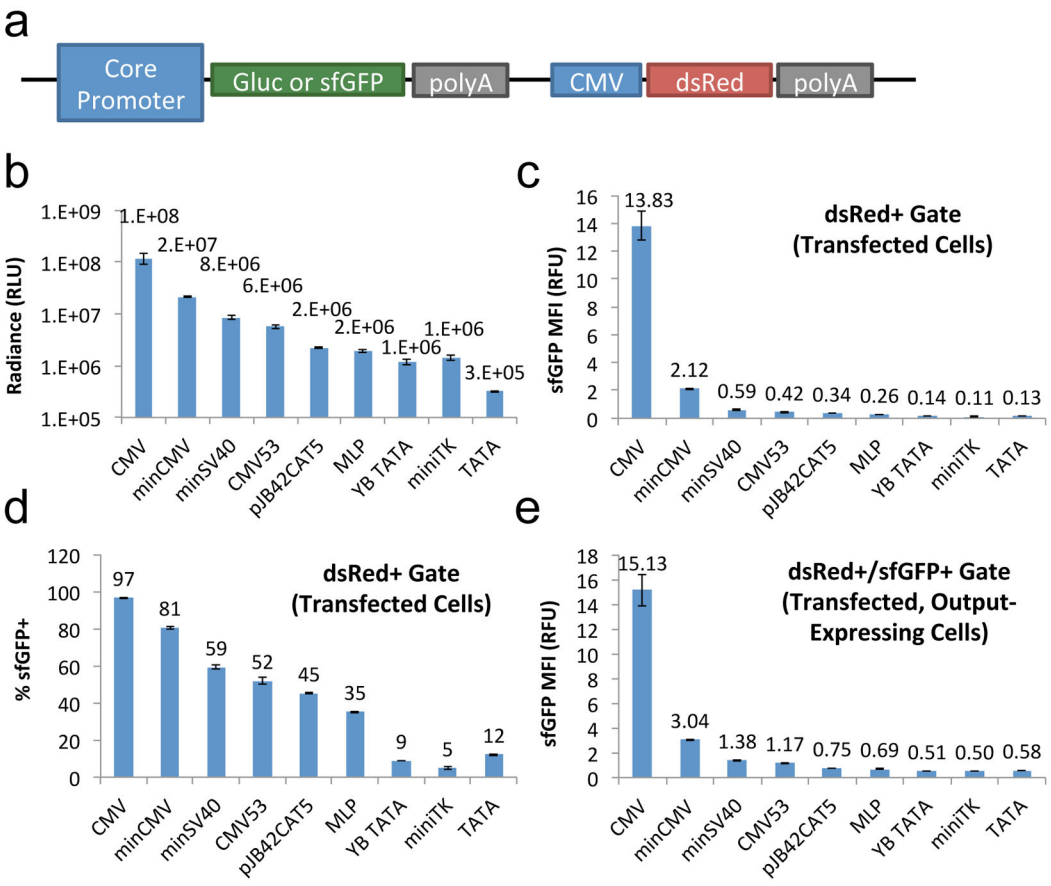

Figure 1.

Panel of core promoters enables a wide range of mammalian gene expression in the uninduced state. (a) Schematic of expression cassette for core promoter evaluation. “PolyA” indicates the bovine growth hormone (BGH) polyadenylation signal. (b–e) HEK 293T cells were transiently transfected with plasmids encoding various core promoters driving the expression of (b) Gluc or (c–e) sfGFP. Each plasmid also encodes for dsRed-Express expressed from a constitutive CMV promoter. (b) Gluc enzymatic activity in culture supernatant reacted with coelenterazine substrate. (c) sfGFP median fluorescence intensity (MFI) among transfected (dsRed+ gated) cells. (d) Percentage of transfected cells that are sfGFP+. (e) sfGFP MFI among dsRed+ and sfGFP+ gated cells. Values shown are the means of triplicates with error bars indicating ± 1 standard deviation (s.d.).

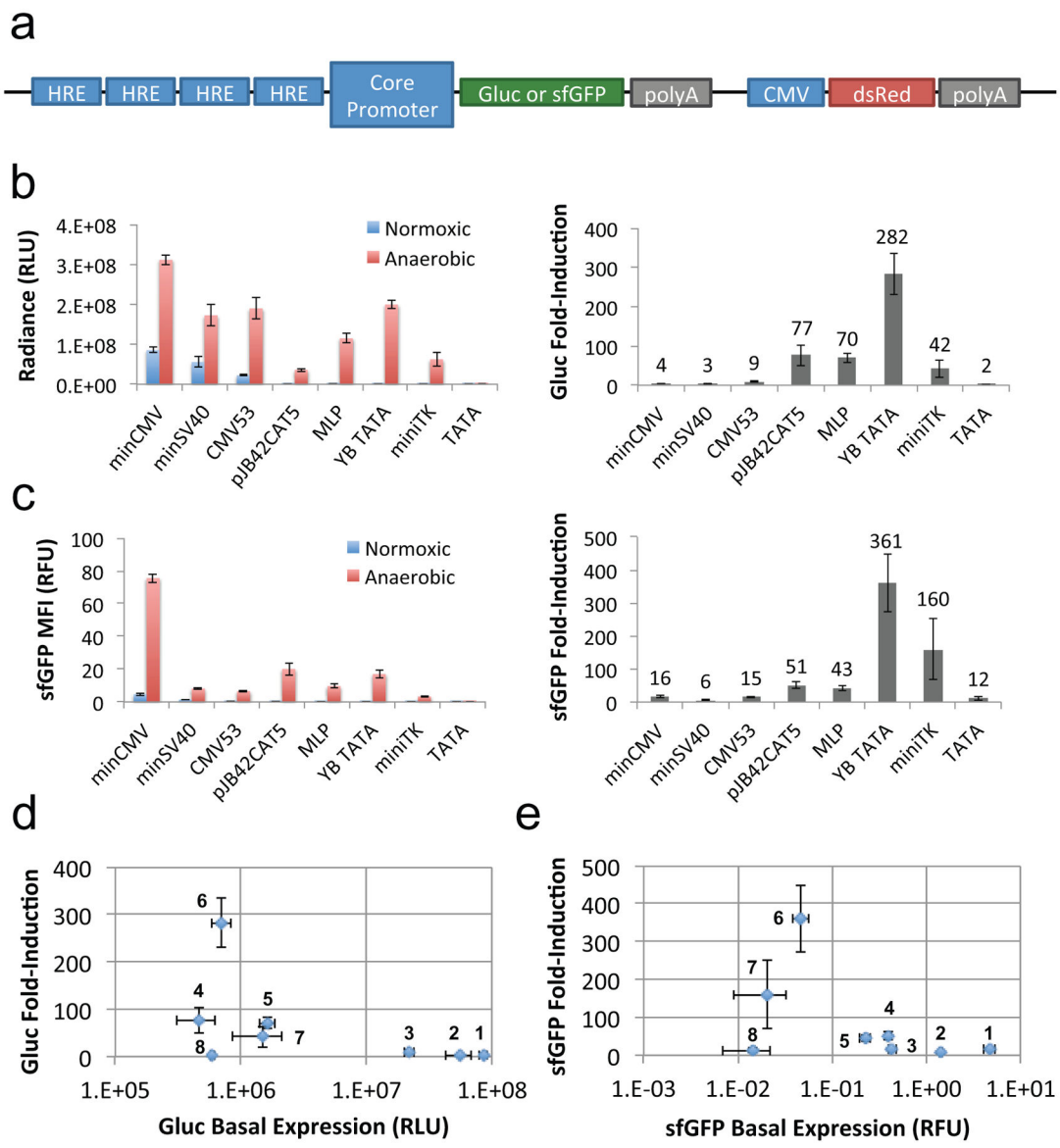

Figure 2.

Core promoter choice is a major determinant of promoter inducibility. (a) Four copies of the hypoxia-responsive element (HRE) were combined with each of eight different core promoters to drive the expression of Gluc or sfGFP. The same plasmid also contains a constitutive CMV promoter that produces dsRed-Express as a transfection marker. Transiently transfected HEK 293T cells were cultured under normoxic or anaerobic conditions. (b) Gluc activity and fold-induction (anaerobic-to-normoxic ratio) in culture supernatant. (c) sfGFP fluorescence intensity and fold-induction among dsRed+ gated HEK 293T cells. (d–e) Fold-induction in (d) Gluc activity and (e) sfGFP fluorescence intensity vs. basal expression. Numbers in (d) and (e) correspond to the following core promoters (from 1 to 8): minCMV, minSV40, CMV53, pJB42CAT5, MLP, YB_TATA, miniTK, and TATA. Values shown are the means of triplicates with error bars indicating ± 1 s.d.

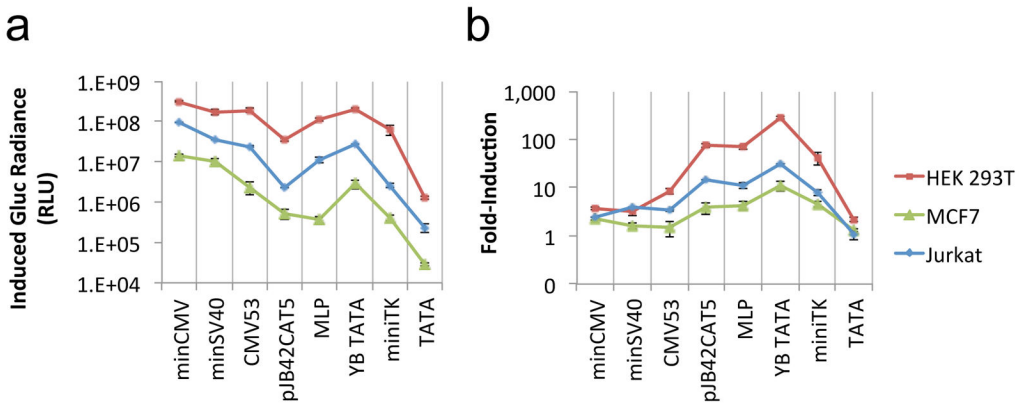

Figure 3.

Relative inducibility of core promoters is consistent across host cell types, with minCMV providing high absolute expression and YB_TATA achieving large fold-change in the induced state. The plasmid constructs shown in Figure 2a encoding Gluc were transiently transfected into HEK 293T, MCF7, and Jurkat cells. Cells were cultured under normoxic or anaerobic conditions. (a) Gluc activity in the supernatant of cells cultured in anaerobic chamber. (b) Fold-induction (anaerobic-to-normoxic ratio) in Gluc activity. Values shown are the means of triplicates with error bars indicating ± 1 s.d.

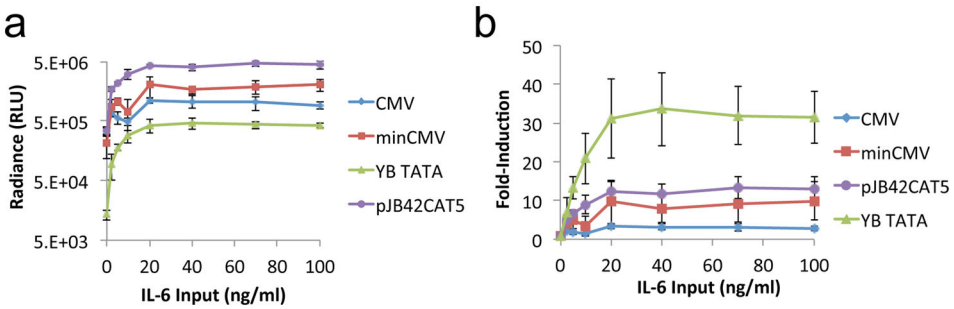

Figure 4.

The induction-response profile of core promoters remains consistent when input signal is changed from hypoxia to IL-6. The JRE-IL6 transcription-factor-binding site was coupled to minCMV, YB_TATA, or pJB42CAT5 and used to express Gluc in transiently transfected HEK 293T cells. The constitutive CMV promoter was included as a reference sample. (a) Gluc activity in supernatant of cells cultured with various concentrations of IL-6. (b) Fold-induction of Gluc activity (normalized to no–IL-6 sample) in cells cultured at various IL-6 concentrations. Values shown are the means of triplicates with error bars indicating ± 1 s.d.

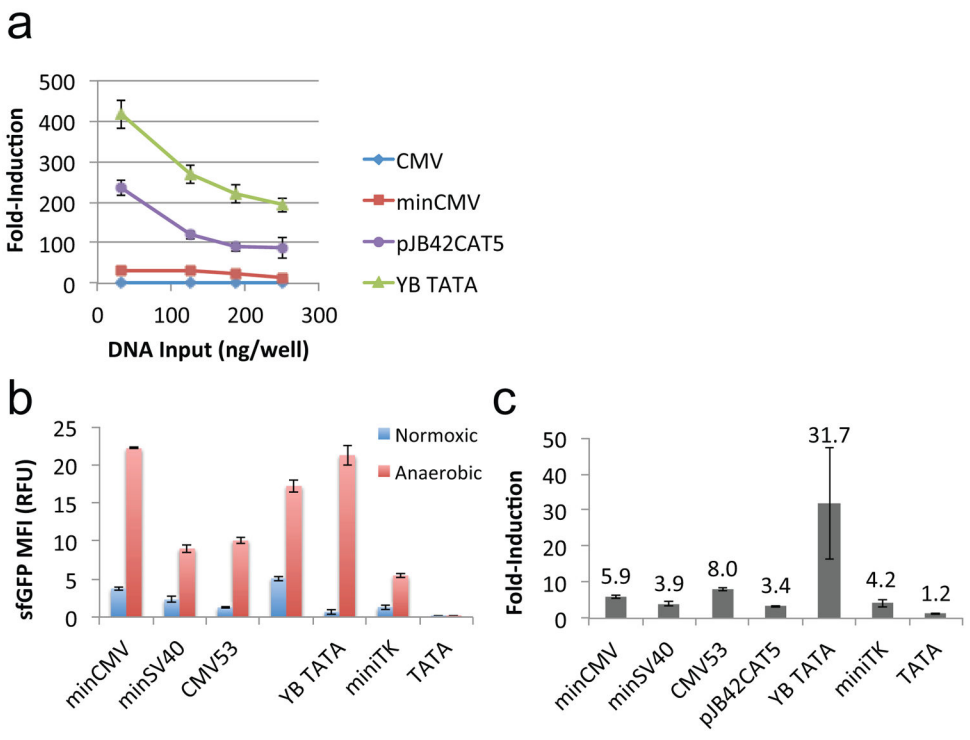

Figure 5.

Relative promoter inducibility is maintained across plasmid copy numbers and upon genomic integration. (a) HEK 293T cells were transiently transfected with various concentrations of the sfGFP-expressing plasmids shown in Figure 2a. Fold-induction was calculated based on median sfGFP intensity among dsRed+ gated cells. (b–c) HEK 293T cells were lentivirally transduced with constructs encoding sfGFP expressed from various hypoxia-inducible promoters. Transduced cells were identified by the expression of EGFRt, which was expressed from a constitutive EF1α promoter encoded in the same lentiviral vector. (b) Median sfGFP intensity of EGFRt+ gated cells was quantified by flow cytometry. (c) Fold-induction was calculated from the data shown in (b). The large error bar for fold-induction of YB_TATA resulted from the fact that this core promoter had very low basal expression (i.e., small denominator in the fold-induction calculation; see Figure 5b). Slight variations in basal gene expression resulted in a large standard deviation in fold-induction after error propagation. Values shown are the means of triplicates with error bars indicating ± 1 s.d.

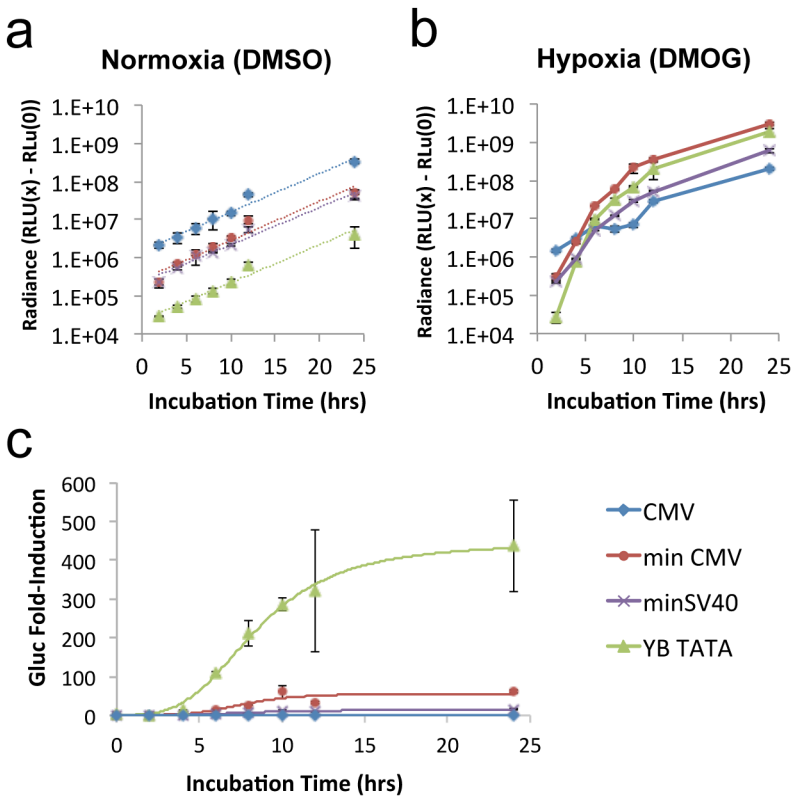

Figure 6.

The synthetic promoter YB_TATA achieves superior fold-induction through combination of low basal expression and high transcription rate in the induced state. HEK 293T cells were transiently transfected with plasmids encoding Gluc expressed from various core promoters coupled to HREx4. Gluc activity in culture supernatant was measured over a 24-hour period. (a–b) Increase in Gluc activity over time under (a) normoxic or (b) hypoxic growth conditions. Radiance values at the 0-hour time point were subtracted from radiance values of subsequent time points to indicate increase in Gluc activity during the induction period. Dotted lines shown in (a) represent regressions fitted for exponential growth. (c) Fold-induction in Gluc activity over time. Experimental data were fitted to the Hill equation; fitted regressions as well as actual data for CMV, minCMV, minSV40, and YB_TATA are shown. All data points shown are the means of triplicates with error bars indicating ± 1 s.d.

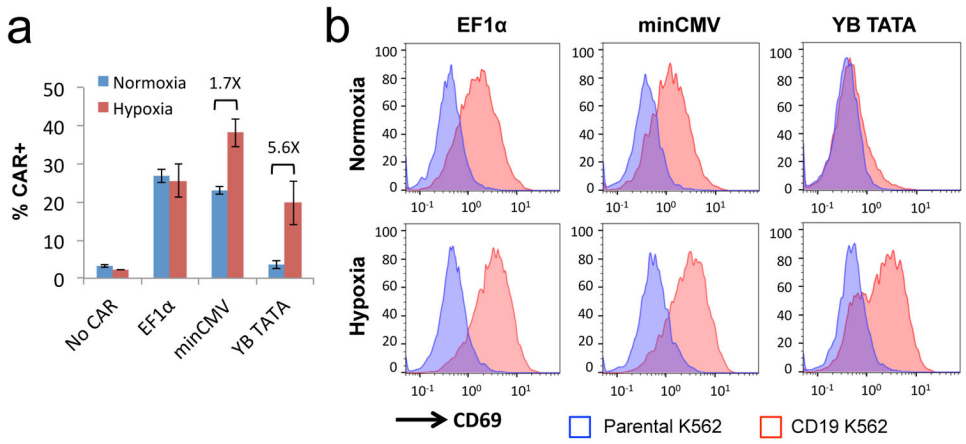

Figure 7.

Proper selection of core promoters enables restriction of antigen-stimulated T-cell activation specifically to hypoxic environments. Jurkat cells were transiently transfected with plasmids encoding a FLAG-tagged CD19 CAR expressed from a constitutive EF1α promoter or hypoxia-inducible promoters featuring either minCMV or YB_TATA as the core promoter. (a) CAR surface expression levels in transfected cells as detected by anti-FLAG antibody staining. Values shown are the means of triplicates with error bars indicating ± 1 s.d. Numbers in the plot indicate fold-induction for minCMV and YB_TATA samples. (b) Jurkat cells were cultured under normoxia for 5 hours post transfection, and then co-incubated with either parental (CD19−) or CD19+ K562 target cells for an additional 24 hours under either normoxic or hypoxic conditions. Expression of the T-cell activation marker CD69 was determined by surface antibody staining. Transfected cells were gated by dsRed+ expression prior to quantification of FLAG or CD69 staining. Data shown in (b) are representative of three independent experiments.